A Retractable Six-Prong Laparoscopic Grasper for Laparoscopic Myomectomy

Brenden Butters[1]
Department of Electrical Engineering and Computer Science,
Massachusetts Institute of Technology,
Cambridge, MA 02139
e-mail: butters@mit.edu

Álvaro Fernández-Galiana[1,2]
Department of Mechanical Engineering,
Massachusetts Institute of Technology,
Cambridge, MA 02139;
Bioengineering Department,
Imperial College London,
London SW7 2BX, UK
e-mail: alvarofg@mit.edu

Daniel Wollin[1]
Integrated Design and Management,
Massachusetts Institute of Technology,
Cambridge, MA 02139;
Division of Urologic Surgery,
Brigham and Women's Hospital,
Boston, MA 02115;
Harvard Medical School,
Boston, MA 02115
e-mail: dwollin@partners.org

Giovanni Traverso
Department of Mechanical Engineering,
Massachusetts Institute of Technology,
Cambridge, MA 02139;
Division of Gastroenterology,
Brigham and Women's Hospital,
Boston, MA 02115;
Harvard Medical School,
Boston, MA 02115
e-mail: cgt20@mit.edu

Alexander Slocum
Department of Mechanical Engineering,
Massachusetts Institute of Technology,
Cambridge, MA 02139
e-mail: slocum@mit.edu

John Petrozza
Department of Obstetrics and Gynecology,
Division of Reproductive Endocrinology and Infertility,
Massachusetts General Hospital Fertility Center,
Boston, MA 02114;
Harvard Medical School,
Boston, MA 02115
e-mail: jpetrozza@mgh.harvard.edu

A Retractable Six-Prong Laparoscopic Grasper for Laparoscopic Myomectomy

The fixation and manipulation of fibroids during laparoscopic myomectomy is a persistent issue for gynecologic surgeons. In this paper, we present a laparoscopic grasper that, through a sheath-based deployment mechanism, opens into a larger multitoothed grasper within the patient and collapses back for removal. Due to the increased number of contact points with the tumor, the expanded grasper allows for reliable fixation, aiding in manipulation during excision. We describe the nature-inspired design of the grasper from a physical foundation, establish the design theory and practical issues, and present manufacturing and testing of a full-scale 5 mm grasper. The unit was tested on synthetic fibroid models and was able to sustain a 50% higher load before tearing than a common single-tooth tenaculum. This development not only promises to improve fibroid fixation in myomectomy but also its design could be adapted to aid in the fixation of other difficult tissues in laparoscopic surgery. [DOI: 10.1115/1.4054013]

1 Introduction

Myomectomy, or removal of benign fibroid tumors of the uterus, is one of the most common gynecologic surgical procedures performed, since women have a cumulative incidence of fibroids between 70% and 80% by age 50 [1]. Minimally invasive surgery is the preferred surgical approach, because the complication and recovery rates are better when compared to traditional open surgery and cosmesis is better [2]. Given the large variety in symptomatic fibroid sizes (from below 0.5 cm to more than 13 cm), fixation and manipulation of these tumors is a difficult challenge during laparoscopic surgery.

Current laparoscopic methods to grasp and mobilize fibroid tumors include the single-toothed tenaculum, toothed forceps (e.g., alligator forceps—Fig. 1), and the myoma screw [3–5]. Studies have documented significant issues with each current

[1]These authors contributed equally to this work.
[2]Corresponding author.
Manuscript received December 6, 2021; final manuscript received March 1, 2022; published online March 31, 2022. Assoc. Editor: Jason Z. Moore.

methodology, including damage to delicate forceps, incomplete or transient grasping with the tenaculum, or bending/breaking of the myoma screw [6–8].

While most gynecologic surgeons who perform laparoscopic myomectomy use standard grasping devices or myoma screws for fibroid fixation, several variations of laparoscopic devices have emerged in recent years. Improvements in standard laparoscopic grasping devices have been focused on force-sensing, decreasing tissue trauma, increased degrees-of-freedom, and more dexterous grasping capabilities [9–12]. Given that myoma-fixation does not suffer from the above issues, these improvements are not particularly relevant to the clinical situation seen during laparoscopic myomectomy.

Improvements in myoma screws have been more common in the academic surgical literature. A myoma screw with a hinged shaft was developed in 1999 and used with good success, allowing for safer lateral traction to the screw and resulting in decreased operative time [5]. The authors noted a decrease in the number of screw insertions per procedure with this hinged shaft device, although these data are not provided. Similarly, one group attempted to resolve the issues with myoma screws by producing an enlarged (10 mm diameter) screw with significant decrease in operative time compared to prior studies [13]. In our experience, many surgeons are not comfortable with the use of the myoma screw in a laparoscopic setting due to frequent bending or breaking, favoring the utilization of the single-toothed tenaculum. For that reason, we focused our efforts on redesigning of the latter. The single-toothed tenaculum is less studied, and although it also suffers to a lesser extent from bending failure issues, its primary drawback is tissue tearing, which also creates the possibility of unwanted tissue dispersion.

Prior work on grasping devices also includes biomimicry inspired design. For many decades, automechanics have had in their tool chest "claw retrievers" [14] which deploy, through a hollow shaft, flexible curved beam "claws" which bend outwards as they exit the end of the hollow shaft. When pulled back in, they inherently close on an object between them. Commercially available medical graspers, often used to retrieve food objects lodged in the throat, function in the same manner and are said to have been inspired by birds of prey (e.g., Talon® [15] and Captura® [16] graspers). However, the grasping based on a flexible member being pulled back into a sheath is defined by the stiffness of the member, which is limited to prevent buckling of the shaft upon deployment. Rigid member graspers (e.g., the Raptor grasper [17]) are frequently used in various surgeries, but these two-prong grasper mechanisms, which are also used in industrial small-part retrieval devices, have been shown to tear through fibroids during myomectomy.

Given these concerns and background, we have developed a three-dimensional laparoscopic myoma-grasping device to allow minimally invasive surgeons a more consistent, straightforward, and robust fixation and mobilization method for fibroid tumors during laparoscopic myomectomy. Its design is also inspired by bird-of-prey talons where we take the approach of true mimicry using three-dimensional rigid members (bones), joints, and tendons (linkage actuation). These animals keep their toes together while approaching their target and it is only before making contact when they fully extend them to form a wide fan of talons, thereby increasing the likelihood of a successful catch. At that point, the bird uses its muscles/tendons to pull on the metatarsus bones, pulling its talons together to achieve a good grip on its prey. Although less glamorous, common birds grasp branches with the same type of mechanism. Likewise, through a sheath-based deployment mechanism, our solution opens into a larger multitoothed grasper only within the patient and collapses back down for removal. Herein, we discuss the modeling, design, and analysis of our device to show the expected improvements over current standard equipment. In the following, we refer to the presented device as the *retractable six-prong laparoscopic grasper (ReSPLaG)*.

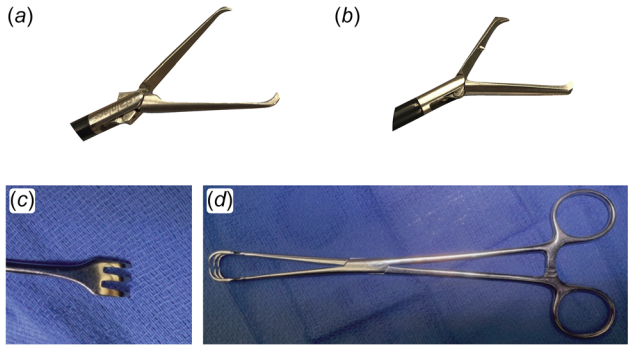

Fig. 1 A variety of surgical grasping devices. (*a*) 5 mm laparoscopic single-toothed tenaculum, (*b*) 5 mm laparoscopic toothed forceps, and (*c*) and (*d*) nonlaparoscopic Pratt tenaculum forceps. In the following, the designs from images (*a*) and (*b*) will be referred to as grasper A and grasper B, respectively.

2 Materials and Methods

2.1 Design Criteria. The major design criteria that influenced the development of the ReSPLaG were the need to maintain a strong grip on the tumor, an ease of repositioning (as frequent regrasping is common), and the need to fit through a 5 mm diameter laparoscopic trocar. Regarding the first criterion, a number of devices are utilized in the traditional open procedure that provide improved grip strength compared to the standard laparoscopic tenaculum. This increase grip is due to such devices not being constrained in their diameter. A device such as the Pratt tenaculum forceps (see Fig. 1) provides a stronger hold on the tumor without tearing through the tissue. While screw-like devices are preferred by some physicians, the propensity of these devices for mechanical failure, as well as the difficulty associated with repositioning, makes them a less attractive model for improvement.

2.2 Prospective Analysis. As discussed, current graspers typically fail by tearing the fibroid tissue during surgeries—due to the concentrated stress on the single jaw. The mechanical homologue of this problem is the stress concentration in notches. This effect has been widely studied for metals and composites, where the stress concentration factors can be computed based on the notch shape. The latter not being true for soft materials and, in particular, for fibroids, makes a jaw shape optimization hard to envision. However, distributing the load over a larger area certainly has a positive impact on the reduction of the localized stress. For this reason, some surgeons prefer the use of Pratt tenaculum forceps, as opposed to regular tenacula, in open myomectomies.

To comply with the dimensional constraint, we designed a foldable device that can be safely introduced through a 5 mm trocar and, once inside the patient, fully deploy into a six-toothed tenaculum, as shown in Fig. 2. During introduction and removal, the foldable device is housed inside a sliding sheath. The side teeth are passively deployed using coil and leaf springs (see Fig. 3). These teeth are collapsed by means of interference with the sheath, as shown in inset (*a*) of Fig. 2.

Once deployed, the actuation of the ReSPLaG tenaculum mimics the actuation of the standard tenacula, but with a larger mechanical advantage. The increased advantage compensates for the larger surface area in contact with the fibroid, thereby maintaining a similar pressure as standard devices. Due to the space required by the spring mechanism, the pulling force as a function of number of teeth follows a diminishing returns law. Taking this into consideration, along with the size of some of the smallest fibroids, a total of three teeth per side were considered for the ReSPLaG. Since the side teeth are placed in a lower plane than

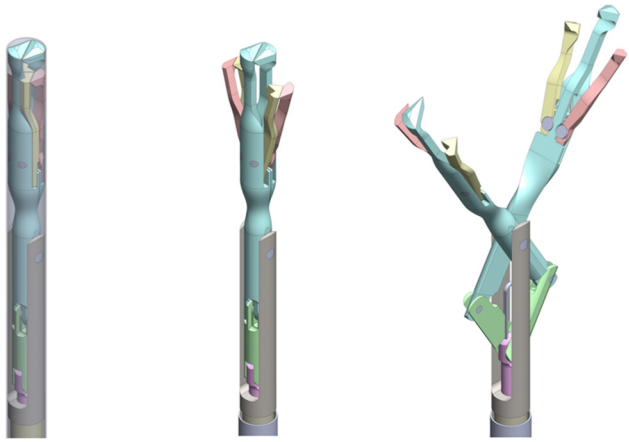

Fig. 2 Rendering of the ReSPLaG design. (*a*) Device in the folded configuration with the sheath extended over the unit. The device is inserted and removed from the patient in this configuration. (*b*) Device with the jaws closed and with the sheath retracted into the operating position. (*c*) Device with the jaws open and all teeth deployed. It is in this configuration that the device would grasp onto tissue.

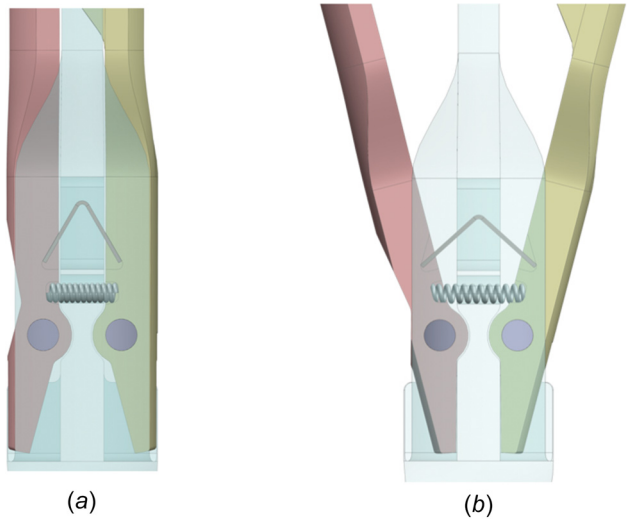

Fig. 3 Rendering of the detail of the miniature springs used for the passive deployment of the side teeth. (*a*) The side teeth are folded into the main body for insertion or removal from the patient. In this configuration, the springs are compressed. (*b*) The side teeth are deployed for operation of the grasper. The springs push the teeth into this configuration when the sheath is slid back. Note that the travel of the side teeth is limited by a tail structure on the bottom of the figure. This maintains a preload on the springs. Note also that the bottom outside of the left tooth has a notch that is not present on the right tooth. This forces the right tooth to close before the left tooth when the sheath is slid over the unit. Thus, ensuring the side teeth will nest correctly within the main jaw.

the main one, their addition does not have an impact on the area of the latter.

The only active actuation is the one required for the grasping action, where a single rod opens and closes the two three-teeth sides symmetrically. A simplified schematic of that actuation mechanism is shown in Fig. 4. The analysis of the linkage establishes that the relationship between the pulling force (H) and the one-jaw grasping force (F) as a function of the half-jaw angle (θ_2) is

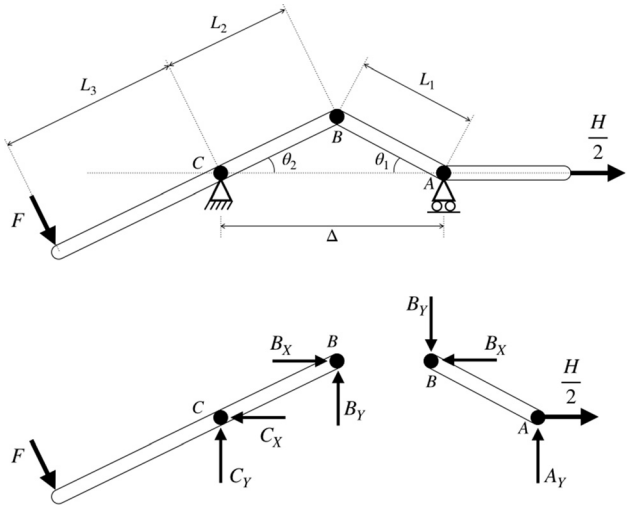

Fig. 4 Diagram of the ReSPLaG actuation mechanism. (Top) The free-body diagram of a single side of the jaw mechanism (the opposing jaw is a mirror of this). The force *F* represents the force exerted by the fibroid on the tooth of the jaw, and the force *H* is the force on the main actuation rod (that is actuated by the handle). (Bottom) A decomposition of the top figure to explicitly show the forces acting on the two members of the actuation mechanism.

$$\left|\frac{F}{H}\right| = \frac{L_2}{2L_3}\sin\theta_2\left[1+\frac{L_2\cos\theta_2}{\sqrt{L_1^2-L_2^2\sin^2\theta_2}}\right]\eta \tag{1}$$

where all the dimensional parameters are shown in Fig. 4, and η is the overall efficiency of the system. This relationship is shown in Fig. 5 for the ReSPLaG, compared with two of the standard laparoscopic tenacula, where the increased mechanical advantage of our design can be observed.

In our design, the intermediate pins (B) are slightly offset from the grasper axis. This offset prevents the angle θ_2 from ever reaching 0, thereby precluding the formation of a geometrical

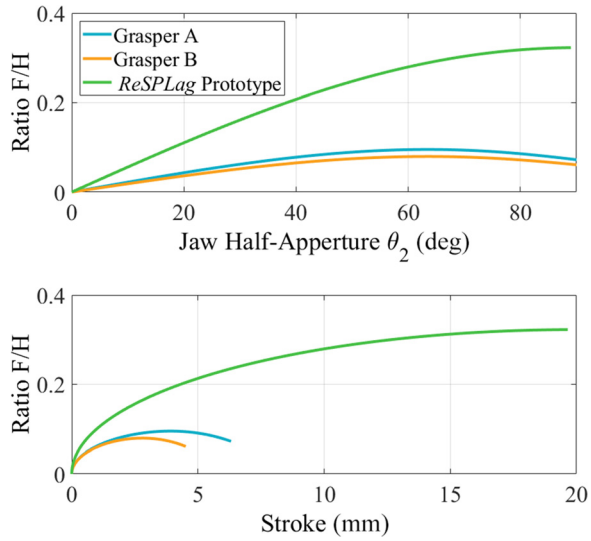

Fig. 5 Mechanical advantage of the ReSPLaG. Ratio of clamping to pulling force for the clamping mechanism as a function of jaw aperture and linear stroke of the actuator. It can be seen that our design achieves a much greater clamping force on the fibroid when for the same force on the actuation rod (and handle) at all angles of the jaws and travel of the main actuation rod.

singularity, where, as shown in Fig. 5, an infinite amount of pulling force is required to produce infinitesimal jaw force.

The calculation used to generate Fig. 5 does not take into consideration the efficiency of our device. To correct for this, the efficiency can be estimated using the friction at the pins. For each pin, the force at the pin is calculated using the diagram in Fig. 4, and the efficiency is

$$\eta = \frac{E_{\text{in}} - E_{\text{loss}}}{E_{\text{in}}} \tag{2}$$

where E_{in} is the energy input to the system from the actuator, and E_{loss} is the energy lost by friction in the pins. We can compute the infinitesimal energy input δE_{in} when the actuator rod is pulled $\delta\Delta$ with force H (note that we use $H/2$ in the calculation since we are only considering one of the two jaws) as

$$\delta E_{\text{in}} = \frac{H}{2}\delta\Delta \tag{3}$$

The energy lost by friction can then be estimated as

$$E_{\text{loss}} = \sum_i \mu F_{\text{pin}_i} R_{\text{pin}_i} \delta\theta_i \tag{4}$$

where μ is the dynamic friction coefficient between the pin and the jaw, F_{pin_i} is the total force held at the pin, R_{pin_i} is the radius of the pin, and $\delta\theta_i$ is the differential angular motion of the pin for a differential actuator motion of $\delta\Delta$. Thus, Eq. (2) becomes

$$\eta = 1 - \sum_i \mu \left(\frac{F_{\text{pin}_i}}{H}\right) D_{\text{pin}_i} \left(\frac{\delta\theta_i}{\delta\Delta}\right) \tag{5}$$

where D_{pin_i} is the pin diameter. For our mechanism, the forces at each pin are

$$F_{\text{pin}_A} = F_{\text{pin}_B} = H\sqrt{\frac{1}{4} + \left(\frac{F}{H}\right)^2 \left(\frac{L_3}{\Delta}\right)^2}, \quad \text{and} \tag{6}$$

$$F_{\text{pin}_C} = H\sqrt{\left(\frac{1}{2} + \left|\frac{F}{H}\right| \sin\theta_2\right)^2 + \left(\frac{F}{H}\right)^2 \left(\frac{L_3}{\Delta} + \cos\theta_2\right)^2} \tag{7}$$

For our grasper, the efficiency has been calculated considering a dynamic friction coefficient of 0.42 and static of 0.78 [18], which has lead to the efficiency curve presented in Fig. 6. Figure 6 shows that, for most of the range of operation, the efficiency is expected to be around 90%. However, as the device approaches full closure, the efficiency quickly decays to zero.

Although the presented analysis is based on simple first principles, it allows us to assess the relevance and implications of the critical geometrical parameters. It is therefore an important tool in the design of the device. In particular, for our device, $L_1 = 10$ mm, $L_2 = 10$ mm, and $L_3 = 31$ mm appear as a good election for a viable design.

With the design foundation complete, we move onto the remaining design requirements. In order to make the use of the device familiar to surgeons, the ReSPLaG is designed to fit in standard handles. As with all re-usable medical instruments, the device must be easily cleaned. To facilitate this operation, the unit was design to be easily separated into parts. Figure 7 is the machined ReSPLaG tip, which is screwed into the actuation rod and the main body of the unit (coaxial rod in tube).

2.3 Device Construction. The prototype ReSPLaG device was fabricated primarily from grade 303 stainless steel rod stock with the small teeth machined from 6Al–4V titanium alloy rod stock. The machining was performed in a vertical machining center (Haas super mini) with a tilt and rotary trunnion for five-axis machining. For details on the construction of the prototype, see

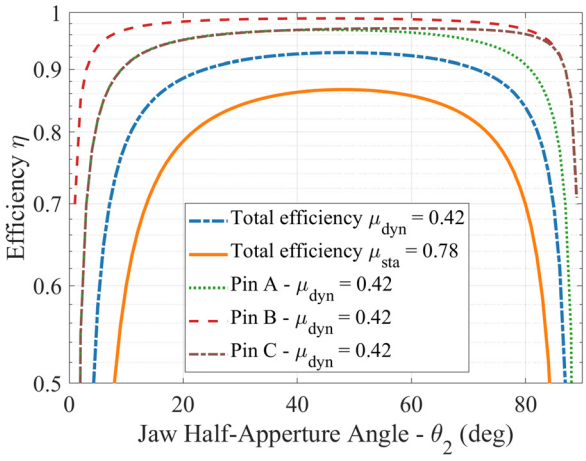

Fig. 6 Computation of the efficiency of our grasper. The efficiency of each individual pin is also computed, which shows that pins A and C are the ones that introduce more loss. The total efficiency is larger that 90% for most of the range, but it drops dramatically when the jaws approach the 0 deg singularity (which our device is prevented from reaching, due to its offset pins).

Appendix A. Once all parts were machined, they were solvent cleaned and sonicated to remove coolant residue prior to welding. With the parts cleaned, each side of the main jaw was assembled with the pins pressed home. The pins were made to be longer than required thus leaving part of the pin protruding on the opposing side. This excess material provided filler material for the otherwise autogenous gas tungsten arc welding that was performed to retain the pins. The parts were welded with a 1/32 in. 2% lanthanated electrode at less than 10 A (foot pedal modulated) with a pulse frequency of 33 Hz, a 10% on-time and 15% background current. Argon back purge was used to prevent oxidation of the reverse side of the parts. In the prototype, the springs are retained by the small side teeth, which necessitates it being in-place when welded. To prevent altering the heat treatment of the spring, one tooth was welded with the other and springs removed. Then, the springs and other side tooth were installed, and the retention pin welded using a higher current and shorter arc duration (to reduce total part temperature). Once the pin welds were complete, the bead was ground down flush with the body of the main jaw. The linkage levers were then installed and, in a similar manner, the clevis pins were welded and ground. The main actuation rod end pins were retained by an interference fit. The unit was then assembled within the yoke, and the main hinge pin installed and welded. Finally, the weld was ground flush. With the assembly complete, the unit was then solvent cleaned. The final device is shown in Figs. 7 and 8.

Fig. 7 Completed ReSPLaG insert prototype. This unit is threaded into the end of the coaxial laparoscopic instrument rod which adapts our design to the standard instrument handle. Actuation of the central rod on the right of the figure opens and closes the jaws of the unit. The unit was designed this way as it facilitates easy cleaning.

Fig. 8 Photograph of the two final prototypes. The unit on the left is open and grasping a grape. The unit on the right is in the collapsed state, as it would be for insertion through a trocar. A U.S. penny is shown for scale.

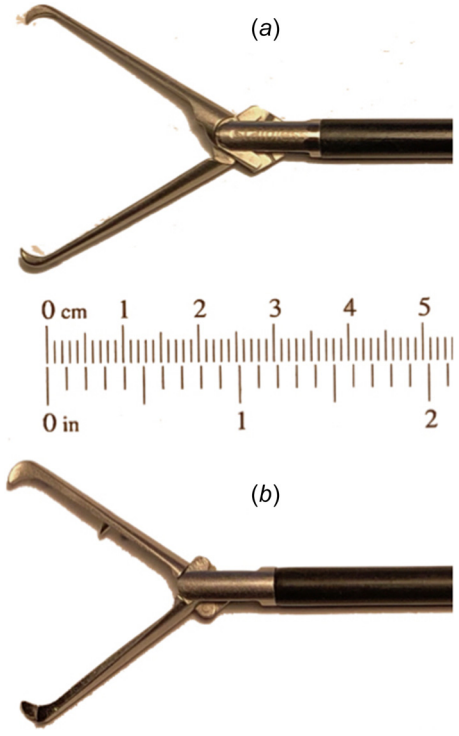

Fig. 9 Detail of graspers A and B (Fig. 1). Both standard commercially available graspers are routinely used in laparoscopic myomectomies. They feature a single main set of teeth that embed within the tissue being grasped. The design B grasper features a second smaller tooth on one jaw that is in line with its main tooth. Neither design features any form of deployable mechanism.

2.4 Device Performance Tests. While exact tissue forces exerted on fibroid tumors during laparoscopic surgery are unknown [8], we developed an in vitro test to inform our design and evaluate the final device performance and to gain qualitative insight about the maximum force before tearing of each of the grasping points. In particular, the test was designed for validation of the completed device in comparison with two standard laparoscopic graspers, see Fig. 9.

In this test, 4 cm × 4 cm × 8 cm coupons of a silicone, chosen for mechanical properties similar to fibroid tissue (Smooth-On Dragon Skin FX-Pro, Macungie, PA) [19], were prepared. These coupons were positioned in the upper grip of a single column universal testing system (Instron, Series 5943, Norwood, MA). The laparoscopic instruments were individually mounted on the lower grip, and 8 mm of silicone was gripped to a homogeneous level of teeth penetration in the silicone. The assembly was then loaded at a rate of

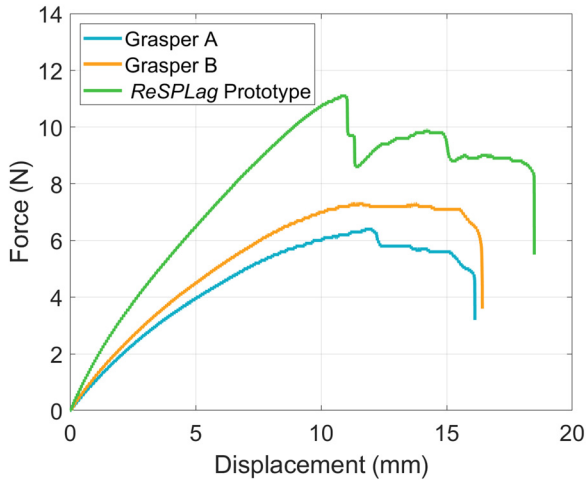

Fig. 10 Typical force–displacement curve for each grasper. The maximum pullout force for the prototype is 50% higher than the best standard grasper. Additionally, when the small extra teeth of our ReSPLaG eventually slip (around 11 mm), and we are only holding with the main jaws, we still maintain a 30% higher force than typical graspers.

15 mm/min, until the point at which it tore or slipped through the silicone coupon. Each test was performed four times with each laparoscopic grasper, and the force–displacement curves were recorded.

3 Results

For each grasper, a total of four test runs were conducted, and all the results were logged. For the full set of results, see Appendix C. Figure 10 shows a typical force–displacement response for each of the graspers that were tested. The results of all tests are summarized in Fig. 11. It can be seen that our prototype substantially outperformed the commercial graspers—obtaining 50% higher tear-out loads. It is important to understand that the results of this test should be interpreted qualitatively and not quantitatively. This is because the mechanical properties of the test silicone do not mimic exactly the behavior of fibroid tissue. Further testing in actual tissue is required to gain quantitative results. That being said, the relatively performance of each design is not expected to change; rather, only the scale of the forces involved.

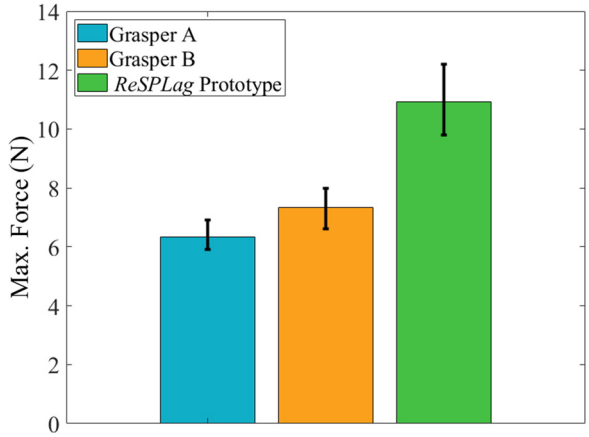

Fig. 11 Comparative maximum force. Results of the maximum force before failure (slipping/tearing of silicone coupon) of each of the graspers tested. It can be seen that graspers A and B performed roughly similar, with grasper B performing slightly better. Our prototype ReSPLaG, on the other hand, substantially out performs the other tested graspers.

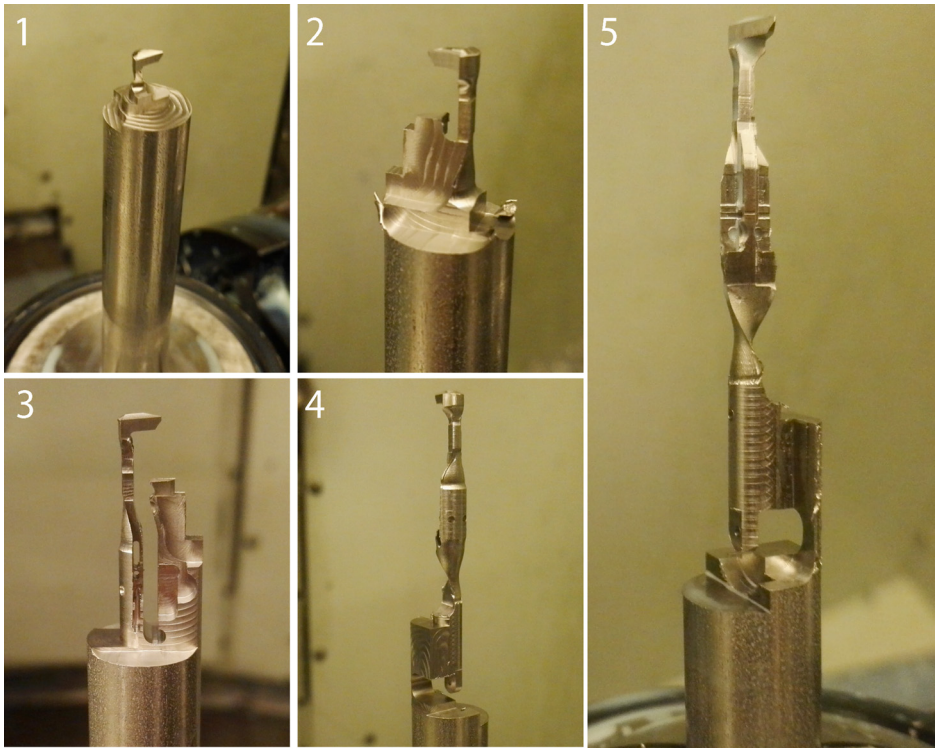

Fig. 12 Typical machining process for the small parts that comprise our prototype grasper. In this case, the part is the main jaw of the grasper. In step 1, the top of the tooth is completed. In step 2, the back of the jaw, and the neck of the main tooth is completed, with the front supported by some remaining support stock. In step 3, the top portion of the part is completed, and the part separated from the support stock. In step 4, the part is almost complete with only the parting operation remaining. In step 5, the part is complete and parted from the parent stock and is only being retained by means of two tabs.

4 Conclusion

To our knowledge, this is the first 5 mm laparoscopic grasper that utilizes a spring-activated mechanism to provide additional jaw spread outside of the standard 5 mm-diameter cross section. Furthermore, this study shows in a preliminary in vitro setting that such a grasper spreads the resultant grasping forces across multiple teeth, thereby providing a higher ultimate tear-out strength when compared to existing devices. We suggest that, by increasing the number of contact points between the grasper and the fibroid, laparoscopic surgeons will be able to more reliably grip the target tumor without concern for tearing of the tissue.

There are a few notable limitations to this study. First, while the silicone chosen for the grasping models matches certain mechanical properties of fibroid tumors, the material is not a perfect replica of the fibrous nature of myoma tissue. Notwithstanding this limitation, we suggest that the relative improvements of the ReSPLaG over the comparison devices seen in these tests are genuine. Additionally, while we machined our device at 1× scale in grade 303 stainless steel and titanium, the comparison devices were fashioned of stronger materials; for this reason, we were unable to test the graspers at true surgical forces or with complete spherical fibroid models. We noted minor deformation of our device at higher forces due to the weaker material in this prototype; future iterations will utilize stronger materials, such as surgical grade stainless steel, to prevent such deformation and allow for more realistic testing forces.

In addition to refinement of material choice, there are a number of future directions for improvements. Optimization of the ReSPLaG for manufacturing and sterilization will be important targets prior to testing in humans. The introducer sheath is currently retracted manually with the use of a second hand—subsequent iterations of the device will allow for retraction of the sheath with the hand that activates the grasping mechanism. Furthermore, the potential for a hinged shaft (to allow for passive flexion along various lateral traction angles) would greatly increase the utility of a grasper that is employed through a single laparoscopic port. This addition would nearly eliminate the lateral forces that are applied to the jaws, thereby making the grasper optimization simpler.

In conclusion, we have presented the design, manufacturing, and testing of a spring-loaded multitooth 5 mm laparoscopic grasping device developed for use in myomectomy surgeries. The "ReSPLaG mechanism" provides increased grasping area and has, in initial in vitro testing, shown an increase in grasping forces prior to tearing on a silicone tissue substitute mode. Further design refinements and testing will aim to bring this project into clinical surgical practice to improve ease and control in laparoscopic myomectomy. Furthermore, the adoption of the innovations brought forth in this paper could greatly assist in the development of instruments for the surgical manipulation of other tissue structures.

Acknowledgment

We would like to thank Mark Belanger, Patrick McAtamney, and the MIT Edgerton Center for their help and for the use of their machines. Dorothy Fleischer and Dave Custer, for their thoughtful comments. Adam Wentworth, for his assistance in device testing. Irina Gaziyeva, Nevan Hanumara, and MIT course 2.75 Medical Device Design,[3] for making this project possible.

Appendix A: Prototype Construction

The full-scale prototype was machined on a five-axis machining center. Each part followed roughly the same process, shown in Fig. 12. Most of the parts were machined from 0.5 in. round bar

[3] https://meddevdesign.mit.edu/

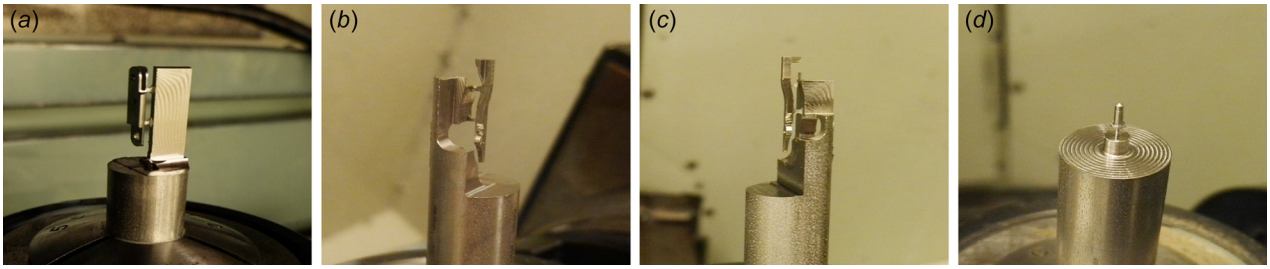

Fig. 13 Completed parts still attached to the parent stock by tabs. The parts are as follows: (*a*) short lever, (*b*) tooth profile a, (*c*) tooth profile b, and (*d*) tooth retention pin. Note: the parts in this figure were test run and were all made in 303 stainless steel (to reduce cost), whereas in the actual prototype parts (*b*) and (*c*) are 6Al–4V titanium.

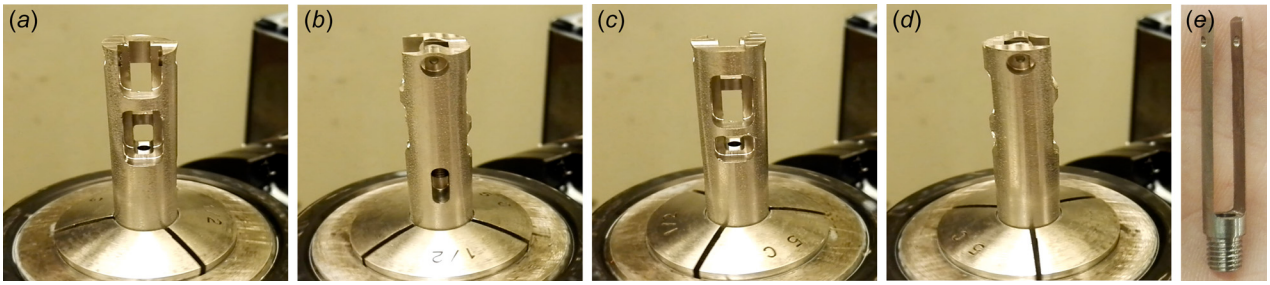

Fig. 14 The yoke was machined in two steps. First, a blank was turned in the lathe and threaded. The blank was then glued into a custom sacrificial mandrel. The mandrel and part were then machined together to form the part shown in (*e*). The completed machining is shown from the (*a*) front, (*b*) right side, (*c*) back, and (*d*) left side.

stock. Such large stock was needed since the spindle on the machine limited how close to the trunnion face the tool could be. Thus, to avoid excessive deflection and chattering, larger stock was required to provide the necessary support (since no pedestal was available for the machine). The part was progressively roughed and finished in stages, such that the amount of unsupported part that was under cutting loads was minimized. This is shown in Fig. 12, where at each stage from 1 to 4, the part is roughed and finished. It can also be seen that material supports were machined into the part, and when they were no longer needed they were parted off. This is seen in step 2, where the material to the left of the jaw supports the jaw while the outside of the jaw is machined. This is then separated from the jaw, see step 3 where the part is free from the support material. In step 4 is can be seen that the, now redundant, support material has been parted off and has fallen away. Finally, in step 5, the part has been parted from the parent stock and is retained by means of two small 0.5 mm tabs on staggered planes to provide rigidity.

A similar process was followed for the other parts, as shown in Fig. 13, with the only difference being the material of the part. The yoke was the only part to be machined differently. Due to its long slender shape, it was necessary to provide support for the part during machining. The direct approach used for other parts would not work here. There were two options, first, machine the part from solid stock with many tabs, which will not give a perfect surface finish and require hand finishing. Alternatively, to turn a blank of the part at its final diameter, thread and bore the actuator pin hole. Then, glue the blank in a custom machined sacrificial mandrel. Then, machine through the mandrel to shape the part inside. When complete, release the glue and remove the completed part. We opted for the latter approach as it made the part programing substantially simpler and reduced the hand finishing required. The completed part within the mandrel and the part after being released from the mandrel are shown in Fig. 14.

In order to retain the pins in their respective locations, each pin is welded into its hole (on one side for all pins other than the main hinge pin which is welded on both sides). Ideally, this would be completed with a laser or electron beam welding process, or at least a plasma welding process. However, with none of these processes available to us at the time of prototype construction, we were left with using a gas tungsten arc welding process. The pins were left long to provide filler material for the welding process, thereby allowing the welding to be otherwise autogenous. This was necessary since providing filler wire to the weld pool would have taken a relatively long period of time. This would have resulted in the parts heating too much, which could alter the heat treat of the springs with where on the opposing side of the pin welds.

Once the teeth were welded to the main jaws, the short levers were installed onto the back of the main jaws. These levers utilize a small clevis with a 1 mm pin. This pin is welded to the body of the clevis on one side. The completed weld is then ground to prevent interference between the weld and other parts. The two sides of the unit are then installed onto the main actuator rod (slip fit). The mostly completed grasper, prior to final assembly and insertion into the yoke, is shown in Fig. 15. Finally, the grasper

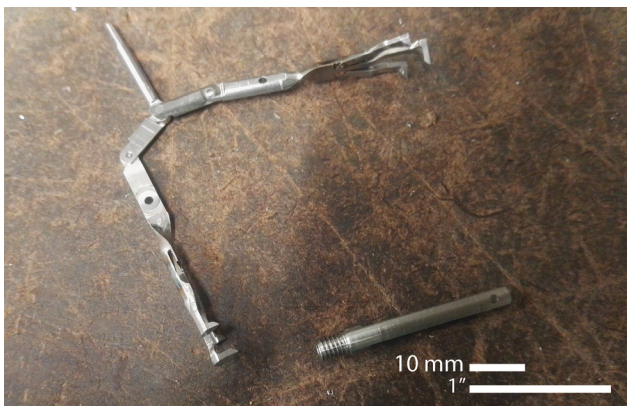

Fig. 15 Completed parts ready for assembly into the yoke and final welding. In this figure, all pins (other than the main hinge pin) have been welded, and the welds ground down. Note: the 1.5 mm main hinge pin is not shown.

mechanism is installed into the yoke, and the 1.5 mm main hinge pin is installed. The pin is welded on both sides of the yoke to prevent the thin yoke from spreading under load. Again, the welds are ground down so that the yoke does not interfere with the sheath. The completed grasper is shown in Fig. 7.

Appendix B: Actuation Mechanism Analysis

The mechanism is described in Fig. 4, and its behavior is studied in Eqs. (1)–(7) and Figs. 5 and 6. The goal of this section is to provide all the equations that yielded those results. We start by solving the forces in the links C and A assuming mass-less bars. We have developed all the calculations as a function of the half-jaw angle (θ_2) and the lengths of the linkages (L_1, L_2, and L_3). This yields to

$$A_y = \frac{L_3}{\Delta} F \tag{B1}$$

$$C_x = \frac{H}{2} + F \sin\theta_2 \tag{B2}$$

$$C_y = F\cos\theta_2 + A_y = F\left(\cos\theta_2 + \frac{L_3}{\Delta}\right) \tag{B3}$$

Note that in the following derivation, the sign convention of each force is shown in Fig. 4. Next, it can be proven that the forces in pin B are equivalent to those in pin A for a mass-less bar. Thus

$$B_x = \frac{H}{2} \tag{B4}$$

$$B_y = \frac{L_3}{\Delta} F \tag{B5}$$

Using all these forces, we can compute the total force at each pin, which corresponds to Eqs. (6) and (7)

$$F_{\text{pin}_A} = F_{\text{pin}_B} = H\sqrt{\frac{1}{4} + \left(\frac{F}{H}\right)^2 \left(\frac{L_3}{\Delta}\right)^2} \tag{B6}$$

$$F_{\text{pin}_C} = H\sqrt{\left(\frac{1}{2} + \left|\frac{F}{H}\right| \sin\theta_2\right)^2 + \left(\frac{F}{H}\right)^2 \left(\frac{L_3}{\Delta} + \cos\theta_2\right)^2} \tag{B7}$$

Note that these forces are only for half of the mechanism. Therefore, each pin is expected to withhold twice the presented values. After solving the free-body diagram, we need to describe the kinematics of the mechanism. Starting by the relationship of Δ with θ_2

$$\Delta = L_1\cos\theta_1 + L_2\cos\theta_2 = L_2\cos\theta_2 + \sqrt{L_1^2 - (L_2\sin\theta_2)^2} \tag{B8}$$

from which we find, after some algebra, the differential motion relationship

$$\frac{\delta\Delta}{\delta\theta_2} = -L_2\sin\theta_2\left[1 + \frac{L_2\cos\theta_2}{\sqrt{L_1^2 - (L_2\sin\theta_2)^2}}\right] \tag{B9}$$

now, using that

$$L_2\sin\theta_2 = L_1\sin\theta_1 \tag{B10}$$

we can write find the following relationship:

$$\frac{\delta\theta_2}{\delta\theta_1} = \frac{L_1\cos\theta_1}{L_2\cos\theta_2} = \frac{\sqrt{L_1^2 - (L_2\sin\theta_2)^2}}{L_2\cos\theta_2} \tag{B11}$$

from which the following relationship can be derived:

$$\begin{aligned}\frac{\delta\Delta}{\delta\theta_1} &= \frac{\delta\Delta}{\delta\theta_2}\frac{\delta\theta_2}{\delta\theta_1} \\ &= -L_2\sin\theta_2\left[1 + \frac{L_2\cos\theta_2}{\sqrt{L_1^2 - (L_2\sin\theta_2)^2}}\right]\frac{\sqrt{L_1^2 - (L_2\sin\theta_2)^2}}{L_2\cos\theta_2} \\ &= -L_2\sin\theta_2\left[1 + \frac{\sqrt{L_1^2 - (L_2\sin\theta_2)^2}}{L_2\cos\theta_2}\right]\end{aligned} \tag{B12}$$

Next, to find the relationship between F and H, we apply conservation of energy, which can be written as

$$FL_3\delta\theta_2 = \frac{H}{2}\delta\Delta \tag{B13}$$

which yields to

$$\frac{F}{H} = \frac{1}{2L_3}\frac{\delta\Delta}{\delta\theta_2} = -\frac{L_2}{2L_3}\sin\theta_2\left[1 + \frac{L_2\cos\theta_2}{\sqrt{L_1^2 - (L_2\sin\theta_2)^2}}\right] \tag{B14}$$

At this point, we have all the information required to compute the forces at the pins as a function of H, which can be used to compute the efficiency. For that, we will use Eq. (5), where the infinitesimal angle displacement for the pins A, B, and C are $\delta\theta_1$, $\delta\theta_1 + \delta\theta_2$, and $\delta\theta_2$, respectively. Figure 16 presents the different geometrical and force relationships for our device.

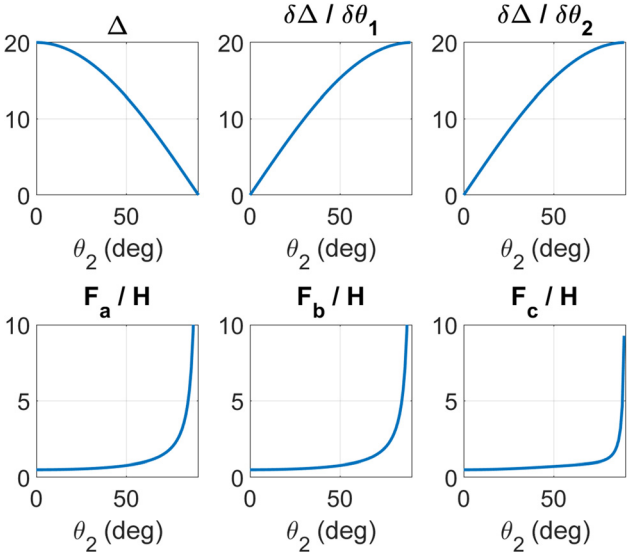

Fig. 16 Relationship between the jaws half-angle (θ_2) and the geometrical parameter Δ, the infinitesimal relationships $\delta\Delta/\delta\theta_1$ and $\delta\Delta/\delta\theta_2$, and the pin forces normalized to the actuation force

Appendix C: Complete Test Data

The complete set of all Instron test results is shown in Fig. 17.

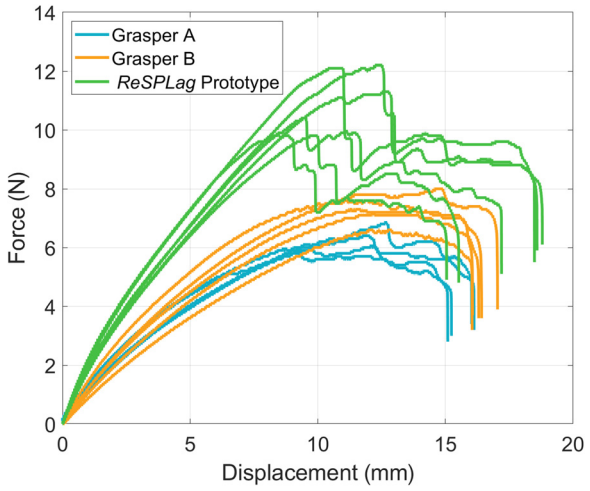

Fig. 17 Complete results from the Instron test. All the instances of testing for each type of grasper are presenter in this force–displacement plot.

References

[1] Baird, D. D., Dunson, D. B., Hill, M. C., Cousins, D., and Schectman, J. M., 2003, "High Cumulative Incidence of Uterine Leiomyoma in Black and White Women: Ultrasound Evidence," Am. J. Obstet. Gynecol., **188**(1), pp. 100–107.

[2] Herrmann, A., and De Wilde, R. L., 2014, "Laparoscopic Myomectomy—The Gold Standard," Gynecol. Minimally Invasive Ther., **3**(2), pp. 31–38.

[3] Takeuchi, H., and Kuwatsuru, R., 2003, "The Indications, Surgical Techniques, and Limitations of Laparoscopic Myomectomy," JSLS, **7**(2), pp. 89–95.

[4] Koh, C., and Janik, G., 2003, "Laparoscopic Myomectomy: The Current Status," Curr. Opin. Obstet. Gynecol., **15**(4), pp. 295–301.

[5] Rossetti, A., Paccosi, M., Sizzi, O., Zulli, S., Mancuso, S., and Lanzone, A., 1999, "Dilute Ornitin Vasopressin and a Myoma Drill for Laparoscopic Myomectomy," J. Am. Assoc. Gynecol. Laparosc., **6**(2), pp. 189–193.

[6] Sinha, R., Hegde, A., Warty, N., and Mahajan, C., 2005, "Laparoscopic Myomectomy: Enucleation of the Myoma by Morcellation While It Is Attached to the Uterus," J. Minimally Invasive Gynecol., **12**(3), pp. 284–289.

[7] Tintara, H., Aiyarak, P., Mitarnun, W., and Geater, A., 2005, "Assessment of the Physical Properties of Laparoscopic Myoma-Fixation Devices," Surg. Endosc., **19**(2), pp. 240–244.

[8] Tintara, H., Aiyarak, P., Mitarnun, W., and Geater, A., 2006, "Effect of Thread Pitch on Pull-Out Strength of Laparoscopic Myoma Screws," J. Obstet. Gynaecol. Res., **32**(4), pp. 428–433.

[9] Schlaak, H. F., Rose, A., Wohlleber, C., Kassner, S., and Werthschutzky, R., 2008, "A Novel Laparoscopic Instrument With Multiple Degrees of Freedom and Intuitive Control," 4th European Conference of the International Federation for Medical and Biological Engineering, ECIFMBE 2008, Antwerp, Belgium, Nov. 23–27, pp. 1660–1663.

[10] Wohlleber, C., and Schlaak, H. F., 2008, "Position Control of Piezoelectric Motors for a Dexterous Laparoscopic Instrument," 4th European Conference of the International Federation for Medical and Biological Engineering, ECIFMBE 2008, Antwerp, Belgium, Nov. 23–27, pp. 1668–1671.

[11] Tholey, G., and Desai, J. P., 2008, "A Compact and Modular Laparoscopic Grasper With Tridirectional Force Measurement Capability," ASME J. Med. Devices, **2**(3), p. 031001.

[12] O'Hanley, H., Rosario, M., Chen, Y., Maertens, A., Walton, J., and Rosen, J., 2011, "Design and Testing of a Three Fingered Flexural Laparoscopic Grasper," ASME J. Med. Devices, **5**(2), p. 027508.

[13] Yoon, H. J., Kyung, M. S., Jung, U. S., and Choi, J. S., 2007, "Laparoscopic Myomectomy for Large Myomas," J. Korean Med. Sci., **22**(4), pp. 706–712.

[14] McMaster, 2020, "Flexible-Shaft Claw Retrievers for Small Parts," McMaster, Elmhurst, IL, accessed Oct. 26, 2020, https://www.mcmaster.com/grippers/flexible-shaft-claw-retrievers-for-small-parts/

[15] Steris, 2020, "Talon® Grasper," Steris, Mentor, OH, accessed Oct. 26, 2020, https://www.steris.com/healthcare/products/endoscopy-devices/foreign-body-management-devices/talon-grasping-device

[16] Cook Medical, 2020, "Captura® Grasper," Cook Medical, Bloomington, IN, accessed Oct. 26, 2020, https://www.cookmedical.com/products/uro_112212udh_webds/

[17] Becton, Dickinson and Company (BD), 2020, "Raptor Grasper," Becton, Dickinson and Company (BD), Franklin Lakes, NJ, accessed Oct. 26, 2020, https://www.bd.com/en-us/products-and-solutions/products/product-page.sp8365

[18] Oberg, E., and Jones, F. D., 1916, *Machinery's Handbook*, Vol. 1916, Industrial Press, South Norwalk, CT.

[19] Jayes, F. L., Liu, B., Feng, L., Aviles-Espinoza, N., Leikin, S., and Leppert, P. C., 2019, "Evidence of Biomechanical and Collagen Heterogeneity in Uterine Fibroids," PLoS One, **14**(4), p. e0215646.